



INSTITUT DE FRANCE
Académie des sciences

Comptes Rendus

Géoscience

Sciences de la Planète

Francesco Vetere, Olivier Namur, Francois Holtz, Renat Almeev, Paola Donato, Francesco Frondini, Michele Cassetta, Alessandro Pisello and Diego Perugini


Influence of volatiles (H₂O and CO₂) on shoshonite phase equilibria

Published online: 19 July 2023

<https://doi.org/10.5802/crgeos.226>

Part of Special Issue: Magma degassing and its impact on the Earth's atmosphere: from magma oceans to lava lakes

Guest editors: Manuel Moreira (Institut des Sciences de la Terre d'Orléans Université d'Orléans-CNRS-BRGM 1a rue de la Férollerie 45071 Orléans France), Bruno Scaillet (Institut des Sciences de la Terre d'Orléans Université d'Orléans-CNRS-BRGM 1a rue de la Férollerie 45071 Orléans France) and Clive Oppenheimer (Department of Geography, University of Cambridge, Downing Place, Cambridge CB2 3EN, UK)

 This article is licensed under the
CREATIVE COMMONS ATTRIBUTION 4.0 INTERNATIONAL LICENSE.
<http://creativecommons.org/licenses/by/4.0/>



*Les Comptes Rendus. Géoscience — Sciences de la Planète sont membres du
Centre Mersenne pour l'édition scientifique ouverte*

www.centre-mersenne.org

e-ISSN : 1778-7025



Magma degassing and its impact on the Earth's atmosphere: from magma oceans to lava lakes

Influence of volatiles (H₂O and CO₂) on shoshonite phase equilibria

Francesco Vetere^{*, a, b}, Olivier Namur^{b, c}, Francois Holtz^b, Renat Almeev^b, Paola Donato^d, Francesco Frondini^e, Michele Cassetta^{f, g}, Alessandro Pisello^e and Diego Perugini^e

^a Department of Physical Sciences, Earth and Environment, University of Siena, 53100, Italy

^b Leibniz University of Hannover, Institute for Mineralogy, Callinstrasse 3, Hannover, D-30167, Germany

^c Department of Earth and Environmental Sciences, KU Leuven, 3001 Leuven, Belgium

^d Department of Biology, Ecology and Earth Sciences, University of Calabria, 87036 Arcavacata di Rende CS, Italy

^e Department of Physics and Geology University of Perugia, piazza Università, 06100 Perugia, Italy

^f Department of Computer Sciences, University of Verona, I-37134 Verona, Italy

^g Department of Industrial Engineering, University of Trento, I-38122 Trento, Italy

E-mails: francesco.vetere@unisi.it (F. Vetere), olivier.namur@kuleuven.be (O. Namur),

f.holtz@mineralogie.uni-hannover.de (F. Holtz),

r.almeev@mineralogie.uni-hannover.de (R. Almeev), paola.donato@unical.it

(P. Donato), francesco.frondini@unipg.it (F. Frondini), michele.cassetta@univr.it

(M. Cassetta), alessandropisello@gmail.com (A. Pisello), diego.perugini@unipg.it

(D. Perugini)

Abstract. Experiments were performed at 500 MPa, 1080 °C and water activities ($a_{\text{H}_2\text{O}}$) from 0.0 to 1.0, in fluid-present and fluid-absent conditions, with the aim of constraining the effect of volatiles on phase equilibrium assemblages of a shoshonite from Vulcanello (Aeolian Islands, Italy). Experiments were run both under reducing and oxidizing conditions and results show that proportions, shapes and size of crystals vary as a function of the volatile composition ($X_{\text{H}_2\text{O}}$ and X_{CO_2}) and volatile content. Clinopyroxene (Cpx) is the main crystallising phase and is compositionally analogous to Cpx crystals found in the natural rock. Plagioclase (Pl) is stable only for water activity lower than 0.1, whereas Fe-Ti oxides are present in all experimental runs, except for those where $\log f_{\text{O}_2}$ was lower than -9, ($\Delta\text{NNO} -0.11$) irrespective of the presence of CO₂. The addition of CO₂ (2.8 wt%) in nominally dry experimental charges substantially reduces the crystallinity by ca. 1/3 compared to volatile free experiments. This result has important consequences upon the physical properties of the magma because it influences its viscosity and, as a consequence, velocity during its travel to the Earth surface.

* Corresponding author.

Assuming that the widths of Vulcanello conduits vary from 0.5 to 1.5 m, estimates of the ascent velocity vary in the range 1.5×10^{-4} – 3.5×10^{-2} m·s⁻¹ for CO₂ free systems and from 5.7×10^{-4} – 1.3×10^{-1} m·s⁻¹ for CO₂ bearing systems.

Since shoshonitic magmas are common not only in the Italian volcanic provinces (Aeolian Arc, Campi Flegrei, Ischia Island, Pontine Islands, Monti Cimini, Monte Amiata, Capraia Island, Radicofani, Roccamonfina) but also in different volcanoes worldwide (Yellowstone, Mariana Arc, Kurile Arc, Tonga Arc, Andean Arc, Kamchatka Arc), we suggest that the new data will be useful to better understand shoshonitic magma behaviour under relevant geological scenarios. As such, we also suggest that hazard evaluation should incorporate the probability of very rapid ascent of poorly-evolved melts from depth.

Keywords. Vulcanello, Shoshonite, Phase equilibria, Mineral assemblage, H₂O–CO₂.

Published online: 19 July 2023

1. Introduction

Volatiles dissolved in magmas are key parameters to understand geophysical and geochemical signals at depth, as their exsolution provides the needed driving force for magma rise and, possibly, trigger explosive eruptions. Being a multiphase system, most magmas are composed of phenocrysts coexisting with a volatile bearing silicate melt (e.g. H₂O, CO₂, S species, F, Cl, etc. . . .). Phase equilibrium studies are of paramount importance to better decipher magma storage conditions and physical properties during ascent to the surface. Thus, the role of parameters governing equilibrium between melt and phenocrysts such as pressure, temperature, redox state, volatile content, must be known. The best way to constrain magma storage conditions of volcanic rocks and changes occurring during ascent is to compare the natural solid assemblages with the phase assemblage and compositions obtained through phase-equilibrium experiments in which all these parameters are controlled [e.g., Martel *et al.*, 2019]. Dissolved volatiles are known to affect the rheological properties of magmas during ascent to the Earth's surface and H₂O is the most important volatile in igneous systems since it affects density, viscosity, as well as phase equilibria, including crystallinity and liquidus temperature [e.g., Burnham, 1981, Schulze *et al.*, 1997]. It is well known that the amount of dissolved water in melts, as well as the mode of degassing in magma conduits, both affect eruptive styles [e.g., effusive vs. explosive, Sisson and Layne, 1992; plinian vs. pelean, Martel *et al.*, 1998].

However, water is not the only volatile component in magmas. Over the last decades researchers have focused their efforts on trying to understand how different volatile ratios, such as H₂O/CO₂, can influence the magma properties in terms of phase equilibria,

mobility of chemical elements, and the amount, shape and size of crystals [e.g. Kent, 2008, Martel *et al.*, 2019, and references therein]. The presence of CO₂ reduces water activity and it is commonly assumed that the decreasing H₂O/CO₂ ratio in the melt results in an increase of the liquidus temperature and crystal/melt ratio in most silicate systems [e.g., Clemens and Wall, 1981, Scaillet and Evans, 1999]. However, the results of some experimental studies seem to indicate that the opposite may occur in basaltic or depolymerized systems at very high CO₂ concentrations (low water activities) [Giuffrida *et al.*, 2017]. These results are unexpected and contrast with our common assumption of the role of CO₂–H₂O-bearing fluids on phase relationships.

In order to expand the experimental dataset on the effect of CO₂ on phase equilibria, we present new H₂O- and CO₂-bearing high temperature and high pressure crystallization experiments performed on a shoshonitic composition from the Vulcanello peninsula (Island of Vulcano, Aeolian Island, Italy). Experiments were targeted to investigate the phase stabilities at pressure and temperature conditions relevant for/to some of the southern Italy volcanoes such as Vulcanello and, possibly, to other chemically similar volcanic systems. We discuss experimental results in terms of phase equilibria but we also address how both H₂O and CO₂ volatiles affect rheological properties of the magma depending on their content.

1.1. *Vulcanello magmatic source and products*

Based on the analysis of fluid inclusions in quartz xenoliths, Zanon *et al.* [2003] provided evidence that the deepest level of magma storage at Vulcanello is located between 17 and 21 km, close to the Moho [21–25 km; Falsaperla *et al.*, 1985] and excluded significant magma ponding at mid-crustal levels. This is

in accordance with the aeromagnetic data at Vulcano pointing to a magma reservoir between 18 and 21 km depth [De Ritis *et al.*, 2013]. Moreover, Zanon *et al.* [2003] provided and estimate for Vulcanello magmas temperature of 1083 ± 40 °C.

The formation of Vulcanello occurred during the last Eruptive Epoch of the island of Vulcano [Eruptive Epoch 8, De Astis *et al.*, 2013], between AD 1100 to 1250 [Arrighi *et al.*, 2006], simultaneously to effusive and explosive activity in the La Fossa crater [Fusillo *et al.*, 2015].

The lava platform comprises several superimposed shoshonitic lava flows, which, together with the products of explosive activity that form a scoria cone, were the first subaerial products of the peninsula (Vulcanello 1). The rocks composing the lava platform are mainly shoshonitic and contain large (up to 1.5 cm) xenocrysts of plagioclase [Davi *et al.*, 2009, De Astis *et al.*, 2013, Fusillo *et al.*, 2015]. After a short time break, the activity resumed with explosive eruptions (Vulcanello 2) which led to the formation of a second cone during a single eruptive unit, showing 3-m-thick fallout deposit having shoshonitic composition [Fusillo *et al.*, 2015]. Following Vulcanello 2, no activity took place during ~500 years. Subsequently, lava emission resulted in the emplacement of the latitic Roveto lava flow, that was followed by three explosive phases leading to the edification of Vulcanello 3 cone. These rocks are latitic in composition with the presence of clinopyroxenes megacrysts [ca. 1.5 cm; Fusillo *et al.*, 2015]. The activity of Vulcanello 3 ended with the emplacement of a final lava flow (Valle dei Mostri latitic lava flow), which flowed in the same direction than the Roveto latitic lava flow [Fusillo *et al.*, 2015, Nicotra *et al.*, 2018, Davi *et al.*, 2009].

2. Experimental and analytical methods

2.1. Starting material and experiments

The starting material of our experiments is a natural scoria lava from Vulcanello 1. The bulk rock composition (Table 1) is characterized by $\text{SiO}_2 = 53.40$ wt% and $\text{Na}_2\text{O} + \text{K}_2\text{O} = 8.76$ wt%. In the total Alkali-Silica (TAS) diagram this composition plots in the field of shoshonite (Table 1). The modal abundance of phenocrysts, mainly composed of clinopyroxene (Cpx) and plagioclase (Pl), is 8–11 vol%.

Table 1. Compositions of starting glass

	VL0 (wt%)	std	Vetere <i>et al.</i> [2007] (wt%)
<i>n</i>	100		100
SiO ₂	53.40	0.41	53.47
TiO ₂	0.70	0.04	0.71
Al ₂ O ₃	15.78	0.24	15.48
FeO	8.04	0.36	8.39
MnO	0.10	0.12	0.10
MgO	4.88	0.15	4.88
CaO	8.81	0.22	8.51
Na ₂ O	3.66	0.23	3.66
K ₂ O	3.71	0.13	4.72
P ₂ O ₅	0.62	0.21	
LOI			
Total	99.76		99.92

Notes: Oxide components are given in wt%. Errors represent one standard deviation (std). Shoshonite studied by Vetere *et al.* [2007] is also reported for comparison.

The phenocrysts often contain inclusions of Fe–Ti oxides. As reported in Davi *et al.* [2009] the composition of clinopyroxene and feldspar phenocrysts ranges between $\text{Wo}_{49-44}\text{En}_{36-42-36}\text{Fs}_{9-20}$ and $\text{An}_{5-46}\text{Ab}_{51-52}\text{Or}_{3-43}$, respectively. Feldspar microphenocrysts show a similar composition to that of phenocrysts ($\text{An}_{3-35}\text{Ab}_{51-61}\text{Or}_{4-46}$). Olivine has a compositional range Fo_{42-62} and the Fe–Ti oxides have Usp content close to 14 mol%. The groundmass consists of glass, leucite (Lc), Fe–Ti oxides, Cpx, Pl and small amount of olivine (Ol).

Sample preparation prior to high-pressure experiments was performed at the Petro-Volcanology Research Group laboratories of the University of Perugia (PVRG; <http://pvrg.unipg.it>). About 100 g of crushed bulk rock was melted in a Pt crucible in air at 1600 °C for 4 h in a Pt₃₀Rh₂₀ crucible. Melting was performed in a Nabertherm HT 04/17 MoSi₂-heated box furnace. The melt was quenched to a glass by pouring it on a brass plate. The glass was crushed, re-melted and quenched again using the same procedure. This technique ensured compositional homogeneity of the glass and avoided crystallization [Vetere *et al.*, 2015a]. The composition of

the glass and the absence of crystals were controlled by electron microprobe imaging and measurements with a CAMECA SX 100 at the Institute of Mineralogy University of Hannover (see details below; Table 1).

The NBO/T parameter corresponds to the number of non-bridging oxygens (NBO) per tetrahedrally coordinated cation (T) and is a good proxy to depict the structure of silicate melts in terms of polymerization [Mysen and Richet, 2005]. This ratio can be calculated as follows:

$$\frac{NBO}{T} = \frac{1}{T} \times \sum_{i=1}^i n \times M_i^{n+} \quad (1)$$

where T is the total atomic abundance of tetrahedrally coordinated cations, M is the proportion of network modifying cations i , with electrical charge $n+$ after subtraction of the portion required for charge-balancing trivalent cations on tetravalent sites [Mysen and Richet, 2005]. Our starting composition has a NBO/T of 0.39. The fragility, F , of our starting composition, was also calculated and has a value of 0.60. This parameter is useful to estimate the deviation from Arrhenian behaviour upon cooling in a plot relating viscosity and the scaled temperature (T_g/T) while approaching the glass transition temperature T_g [Angell, 1995, Giordano and Dingwell, 2003]. Both the NBO/T and F point to a high degree of depolymerisation of our starting material.

In order to prepare volatile-bearing charges, we used the following procedure:

The capsules ($Au_{80}Pd_{20}$; 5 mm diameter, 3 cm in length, previously annealed at 1100 °C for 10 min and then welded on one end) were filled with the following procedure: (a) the capsule was charged with the desired amounts of $\pm H_2O \pm Ag_2C_2O_4$ + glass powder ($Ag_2C_2O_4$ is the source for CO_2 as the silver oxalate decomposes during heating and generates the carbon dioxide); (b) a steel piston was used to gently compact the charge; (c) to avoid any volatiles release, the capsule was tightly squeezed on top, rolled up in a wet tissue, and frozen by placing it into a bath of liquid nitrogen; (d) the upper end of the capsule was welded shut with a conventional graphite-arc welder. In agreement with literature data on the Vulcanello magmatic source (21–17 km depth and 1083 ± 40 °C, see above) we performed experiments at 500 MPa and 1080 °C for 70 h, in order to shed light on processes relevant to the magmatic source of Vulcanello magma.

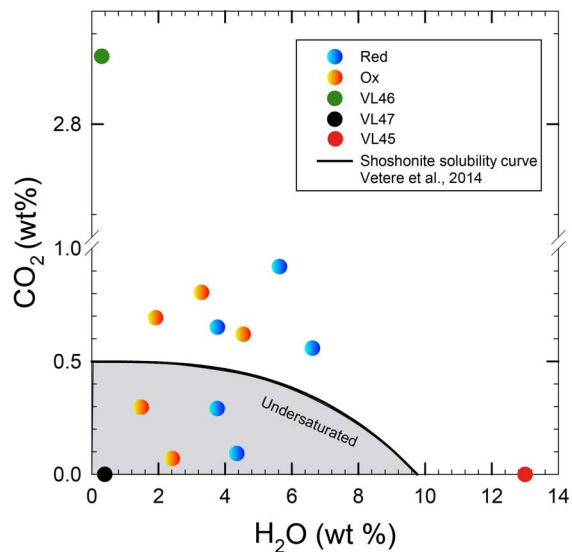


Figure 1. H_2O and CO_2 concentrations added to the capsules before experiment (at 500 MPa and 1080 °C). The shaded area represent the undersaturated conditions in accord with the modeled H_2O and CO_2 concentrations at fluid saturation obtained by Vetere *et al.* [2014, 2011] for the same composition is also shown (solid black curve). Orange and blue symbols indicate experiments performed at reduced and oxidized conditions, respectively, (see Table 3). Green and black circles are nominally anhydrous VL46 and 47 experiments, respectively (Table 3). Red dot refers to the sample with the highest water content.

A total of 13 experiments with variable volatile contents (see Figure 1) were performed at 500 MPa and 1080 °C (Tables 2 and 3). Experiments were done in an internally heated pressure vessel (IHPV) equipped with a rapid-quench sample holder at the Institute für Mineralogy, Leibniz University of Hannover (Germany). Details for the IHPV are provided in Berndt *et al.* [2002]. Temperature was measured using four unsheathed S-type thermocouples (precision of temperature was ± 5 °C). The IHPV was pressurized with argon. Pressure was monitored

Table 2. Results of microprobe analyses of residual glasses

	VL32	std	VL33	std	VL34	std	VL36	std
SiO ₂	54.86	0.39	55.53	0.47	54.28	0.60	52.17	0.55
TiO ₂	0.71	0.05	0.73	0.04	0.73	0.06	0.71	0.04
Al ₂ O ₃	20.61	0.26	20.71	0.34	19.87	0.22	17.99	0.23
FeOT	1.81	0.57	1.21	0.27	1.99	0.31	2.95	0.18
MnO	0.10	0.06	0.09	0.04	0.15	0.09	0.13	0.11
MgO	1.72	0.15	1.51	0.57	2.13	0.37	3.07	0.46
CaO	4.70	0.31	4.13	0.27	5.16	0.27	6.23	0.10
Na ₂ O	6.32	0.26	6.66	0.16	6.08	0.21	5.42	0.17
K ₂ O	4.91	0.39	5.11	0.21	4.82	0.28	4.25	0.32
P ₂ O ₅	0.49	0.14	0.56	0.21	0.45	0.10	0.46	0.16
Total	96.23		96.24		95.66		93.38	
H ₂ O	3.77		3.76		4.34		6.62	
	VL37	std	VL38	std	VL39	std	VL41	std
SiO ₂	55.50	0.68	56.03	0.47	55.72	0.91	53.90	0.21
TiO ₂	0.45	0.13	0.49	0.10	0.49	0.09	0.62	0.05
Al ₂ O ₃	20.35	1.03	20.67	0.62	20.18	0.72	18.57	0.27
FeOT	4.32	1.07	4.12	0.70	3.96	0.58	4.64	0.23
MnO	0.12	0.05	0.09	0.10	0.09	0.10	0.10	0.11
MgO	1.29	0.38	1.14	0.23	1.10	0.32	2.00	0.37
CaO	3.99	0.40	3.69	0.42	3.60	0.32	4.66	0.17
Na ₂ O	6.65	0.35	6.74	0.38	6.95	0.17	5.87	0.10
K ₂ O	4.86	0.27	5.04	0.24	5.07	0.26	4.65	0.18
P ₂ O ₅	0.57	0.23	0.51	0.16	0.50	0.17	0.46	0.12
Total	98.10		98.52		97.66		95.47	
H ₂ O	1.90		1.48		2.34		4.53	
	VL45	std	VL46	std	VL47	std		
SiO ₂	51.36	0.99	56.02	0.83	55.69	0.44		
TiO ₂	0.63	0.02	0.76	0.02	0.75	0.04		
Al ₂ O ₃	15.01	0.24	18.10	0.34	18.55	0.64		
FeOT	7.29	0.41	7.15	0.46	6.75	0.41		
MnO	0.10	0.10	0.13	0.08	0.18	0.09		
MgO	4.19	0.29	2.40	0.10	2.23	0.39		
CaO	7.34	0.44	4.33	0.12	4.48	0.66		
Na ₂ O	2.81	0.39	6.07	0.26	6.21	0.20		
K ₂ O	3.61	0.13	4.01	0.08	4.01	0.27		
P ₂ O ₅	0.51	0.04	0.74	0.03	0.75	0.07		
Total	91.85		99.70		99.61			
H ₂ O	8.15		0.30		0.39			

Notes: H₂O represent the water content estimated by difference methods. Microprobe data are reported for all the residual glasses investigated in wt% together with errors represented by one standard deviation (std).

Table 3. Phase assemblage results derived from image analyses methods

	H ₂ O _{in} (wt%)	CO ₂ (wt%)	$a\text{H}_2\text{O}^{\text{f}}$	$\log f\text{O}_2$	ΔQFM	CPx			Plg			Ox	Φ_{tot} (area%)	
						Fs	Wo	En	An	Or	Ab			Φ_{Plg} (area%)
VL32 [#]	3.5	0.651	0.36	-10.80	-1.37	17.31	46.40	36.28	16.1					16
VL33 [#]	3.5	0.291	0.35	-10.82	-1.39	13.25	47.03	39.71	16.3					16
VL34 [#]	4.2	0.092	0.44	-10.64	-1.21	16.11	45.87	38.00	14.3					14
VL35 [#]	5.5	0.919	0.61	-10.35	-0.92				10.7					11
VL36 [#]	6.5	0.558	0.74	-10.18	-0.75				10.2					10
VL37	2.0	0.693	0.14	-7.64	1.79				15.8				1.7	17
VL38	1.5	0.297	0.09	-8.01	1.42				18.1				1.7	22
VL39	2.5	0.070	0.19	-7.38	2.05				18.7				1.9	21
VL40	3.0	0.805	0.31	-6.94	2.49	15.67	41.34	42.96	17.0				1.5	18
VL41	4.5	0.620	0.48	-6.57	2.86	16.45	47.85	35.68	14.0				1.4	15
VL45 [§]	13.0	0.000	1.00	-4.94	4.49									3
VL46*	0.0	2.830	0.01	-10.26	-0.83	17.33	42.91	39.75	15.3	33.58	9.60	56.82	5.9	21
VL47*	0.0	0	0.02	-8.92	0.51	17.90	42.42	39.68	21.6	32.91	9.40	57.69	8.8	30

Crystals composition are also reported.

Note: Crystallinity (Φ) is reported in vol% and derived from 500 MPa and temperature of 1080 °C experiments. H₂O and CO₂ are reported in wt%. Water activity is also reported for all run while phase compositions are reported for most of the experimental runs except for those were crystal size was too small in order to be analyses. [#]Denote experiments performed at controlled $f\text{O}_2$. *Denote experiments were no water was added to the charges. [§]Denote experiments with quench crystals. [†]Water activity is calculated from the amount of water estimated by the difference method (see Table 2).

using digital pressure transducers having an uncertainty of about 1 MPa. The variation of pressure during the experiments was ≤ 5 MPa. Some experiments were performed at the intrinsic oxygen fugacity (f_{O_2}) conditions of the pressure vessel which was found to be close to QFM+4 (the intrinsic f_{O_2} corresponding to H_2O -saturated conditions), with QFM being the quartz–fayalite–magnetite equilibrium [Berndt *et al.*, 2002]. At H_2O -undersaturated conditions, f_{O_2} is lower, depending on the prevailing water activity [QFM–0.8 to QFM+3; Botcharnikov *et al.*, 2005]. In our experiments f_{O_2} was calculated using the following relation:

$$\log f_{O_2} = \log f_{O_2}(\text{at } X_{H_2O_{in}} = 1) - 2 \log X_{H_2O_{in}}. \quad (2)$$

[Scaillet and Evans, 1999]. We estimate that the maximum error on the calculated f_{O_2} is about 0.2–0.3 log units according to Botcharnikov *et al.* [2005]. Other experiments were performed under controlled f_{O_2} conditions (QFM–0.7 to QFM–1.4) by adding H_2 to the Ar pressure medium. The hydrogen fugacity (f_{H_2}) in these experiments was monitored using a Shaw membrane as described in Berndt *et al.* [2002]. The f_{H_2} was adjusted to be $f_{H_2} = 20$ bar at experimental P–T conditions. Experiments were drop quenched with a cooling rate of approximately 150–200 °C/s [Berndt *et al.*, 2002]. For one experiment (Table 3), it was not possible to avoid the formation of quench crystals due to the relatively high amount of added water (see results for details).

2.2. Electron microprobe and image analyses

All run-products were mounted in epoxy, ground flat and polished for textural and chemical analyses. Glasses and minerals produced during the experiments were analysed using a Cameca SX100 microprobe at the Institute of Mineralogy. An accelerating voltage of 15 kV was used with a beam current of 15 nA for silicate minerals and oxides and 6 nA for glasses. The beam was defocused to at least 15 μm for glass analyses and focused to < 2 μm for the analysis of crystal phases. All elements were analysed with a counting time of 10 s on peak. Standards used for calibration were Fe_2O_3 , MgO, $MnTiO_3$ (Mn and Ti), albite (Na), wollastonite (Si for mineral and glass and Ca for glass), apatite (P and F for glass and F, Ca and P for apatite), orthoclase (K), anhydrite (Ca and S). Standard deviations reported in Table 2 were

calculated based on 10 to 20 analysed spots on the same sample. Raw data were corrected with the software “Peak Sight” and “PAP” matrix [Pouchou and Pichoir, 1991]. Precision and accuracy were determined by measuring reference glasses VG-568 (rhyolite) and VG-2 (basalt) from Smithsonian standards collection [Jarosewich, 2002].

Due to the presence of crystals in experimental charges, the water content of the glasses was estimated following the “by-difference” method described in Devine *et al.* [1995]. Following Parat *et al.* [2008], we estimate that the error on determination of H_2O content is ~ 0.5 wt%. CO_2 in glasses were not determined but estimated from the solubility curve in Figure 1.

Back-scattered electron (BSE) images were collected with a Philips FEG (Field Emission Gun) Quanta 200F equipped with a Si/Li-SUTW detector (EDAX, Philips Electronics) installed at the University of Calabria (Italy). Representative BSE images were collected at different magnifications (400 \times up to 1600 \times) depending on the crystal size. Surface percentage of the different phases was determined for all images using grey levels with Image-ProPlus 6.0 [see details in Vetere *et al.*, 2015a]. Seven to ten BSE images obtained in different parts of the same section were evaluated for homogeneity. We quantified surface fractions of glass, clinopyroxene, spinel, plagioclase and gas bubbles. In total, 110 BSE images were analysed.

3. Results

The crystalline phases observed in our experiments are clinopyroxene (Cpx), plagioclase (Pl), and Fe–Ti oxides (Ox) in various proportions, depending on the fraction of volatiles dissolved in the melt. The results show that Cpx is the main phase with abundance increasing from 10.2% to 21.6% as a_{H_2O} decreases from 0.74 to nearly zero (Table 3). Water activity also plays a major role on the stability of Pl that is only present in experiments with a melt H_2O content ≤ 1 wt% (Table 3). Plagioclase has a maximum abundance of 8.8% in the volatile-free sample (VL 47* in Table 3). Minor Fe–Ti oxides ($\leq 2\%$) are present in samples equilibrated under relatively high oxygen fugacity conditions.

Based on the amounts of added volatiles and in agreement with solubility model and data

[e.g. Vetere *et al.*, 2014] one can distinguish between fluid-saturated (fluid present) and fluid-undersaturated (fluid absent) runs with respect to $\text{H}_2\text{O} + \text{CO}_2$ (Figure 1).

Quenched melt (residual glass) is present in all run products with a mode ranging from 70% in VL47* to 97% in VL45^s (Table 3). This wide range of melt fraction at constant pressure and temperature shows the importance of water activity ($a\text{H}_2\text{O}$) on the liquidus temperature and crystallinity. All glass compositions, including the starting composition, are listed in Tables 1 and 2 and are illustrated in Figure 2. The compositions of residual glasses range from 51 to 56 wt% SiO_2 (Table 2 and Figure 2). Glass compositions evolve as a function of the degree of crystallinity. We however note that a larger crystallinity does not always correspond to an enrichment of SiO_2 in the residual glass (compare Table 2 and 3). We also note that in the experiment performed under oxidizing and water-saturated (no CO_2) conditions, the conditions are close to the liquidus and the melt has a composition very similar to that of the starting glass (although comparing alkali content in the VL45 and starting material we do note a difference of ca. 0.5 wt% of Na_2O possibly due to the EPMA measurements conditions; red point in Figures 1 and 2). Experiments performed at reducing conditions and containing both water and CO_2 show a SiO_2 trend that increases nearly linearly as the MgO content decreases. The same observation can be done for, Na_2O and K_2O . The total FeO decreases with decreasing MgO but FeO concentrations are always higher in oxidized experiments than in reduced experiments at a given MgO content, suggesting a possible Fe-loss to the capsule wall at reducing conditions, as discussed below. TiO_2 is relatively constant in reduced experiments but decreases with decreasing MgO in oxidized runs. Due to the crystallization of the main phase Cpx, CaO continuously decreases with MgO (with increasing crystallinity).

Eight experiments were performed at volatile saturated conditions and six at volatile undersaturated conditions (Figure 1). Figure 3 shows the variation of crystal content as a function of water content. The general trend indicates that the higher the amount of water in the melt, the lower the amount of crystals, as expected from the numerous previous phase relationships conducted so far. No significant difference between fluid-absent and fluid-present runs

is detected in terms of crystal content in samples with an amount of water added to the system that is larger than 1.0 wt%. Thus, we did not detect a substantial difference in crystal content between experiments performed at fluid-saturated and fluid-undersaturated conditions if the $a\text{H}_2\text{O}$ is similar. For example, we investigated the effect of increased CO_2 concentration in water-rich samples (i.e. up to 3.7 wt% H_2O ; sample VL32 and VL33, see Table 3) by performing two experiments with a total amount of CO_2 from 6500 ppm (fluid-saturated) and 2900 ppm (fluid-undersaturated). No difference between CO_2 -rich and CO_2 -poor samples was observed in terms of crystallinity. In particular, both melts showed Cpx contents of ~16% (Table 3). In contrast, our experiments show that, at very low H_2O content, the presence of CO_2 causes a substantial decrease of crystal content. A difference up to 10 area% in crystal content is observed between samples VL46 and VL47 (see Table 3), where the first charge contains a large amount of CO_2 (2.8 wt%, nominally dry, no water added) while VL47 is nearly volatile free. It is emphasized that this difference of 10 area% in crystallinity determined by image analysis is also consistent with mass balance calculations. Using the GeoBalance program [Excel VBA program for mass balance calculation; Li *et al.*, 2020] the residual melts in VL47 can be best reproduced if 6 wt% Pl and 30 wt% Cpx crystallize from the starting material (the mineral compositions from experimental products were considered for the calculation, see Table 3). For VL46, mass balance calculation indicates the crystallization of 3 wt% Pl and 25 wt% Cpx, pointing to the possible role of CO_2 on phase proportions as discussed below.

The alphaMELTS code was used to further elucidate the phase evolution observed in this study. The alphaMELTS (V. 1.9) software provides a simple text-based interface to subroutine versions of the algorithms MELTS [Asimow and Ghiorso, 1998, Smith and Asimow, 2005, Ghiorso *et al.*, 2002, Ghiorso and Sack, 1995]. It allows to calculate equilibrium assemblages along a thermodynamic path set by the user (details are provided by: <http://melts.ofm-research.org/> and <https://magmasource.caltech.edu/forum/>). Results of the simulations are shown in Figure 4 comparing the crystals content measured via Image Analyses and calculated by using alphaMELTS. There is a good correlation between calculated and measured

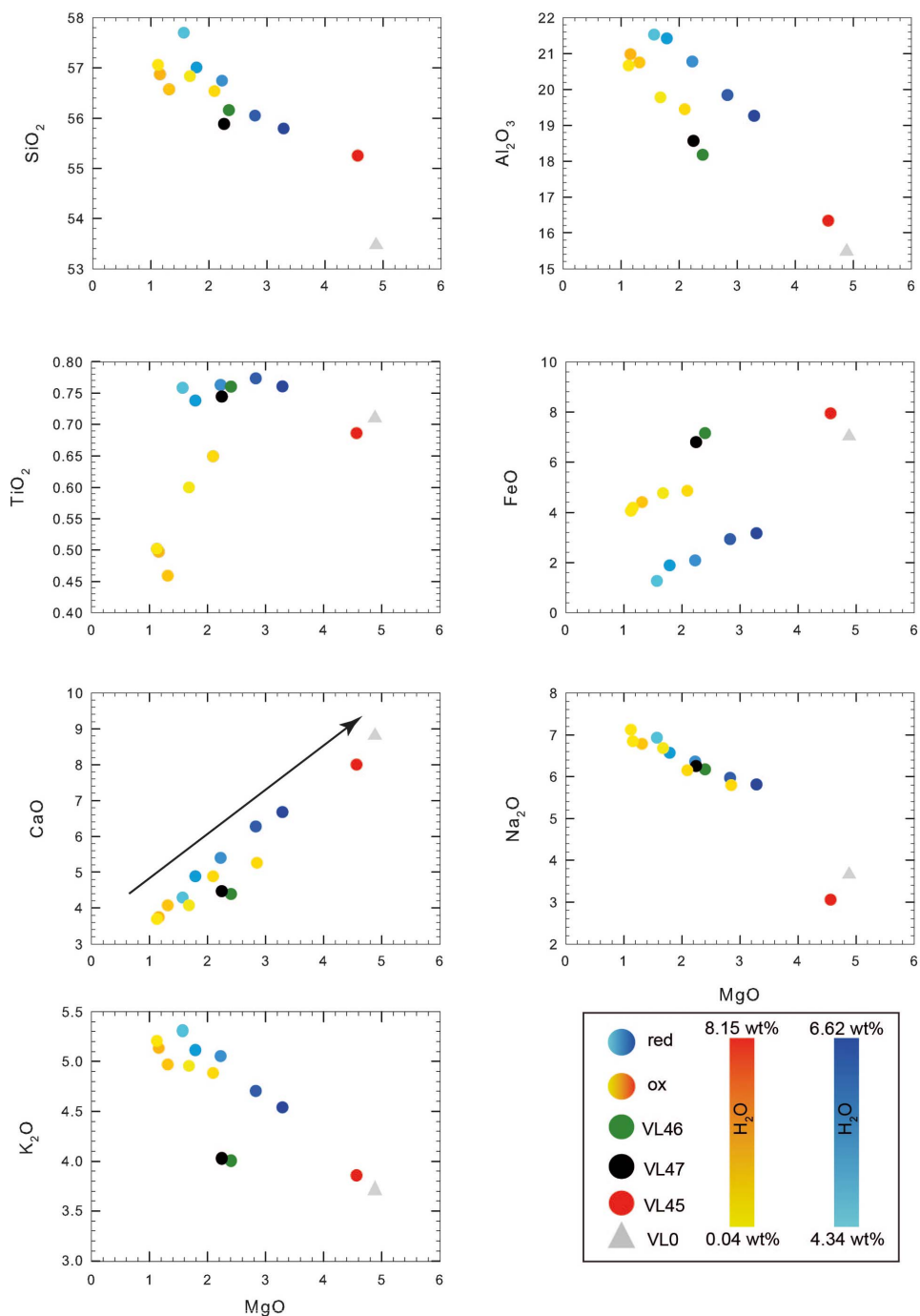


Figure 2. Change of the residual glass composition (in wt% of element concentrations) in the silicate melts. The analyses are recalculated to a total of 100%. The arrow on the CaO vs. MgO plot indicates the vector pointing to the Cpx composition. The grey triangle refers to the starting material composition while reddish and bluish circles indicate experiments performed at oxidized and reduced conditions, respectively, as reported in Tables 2 and 3. Red dot as in Figure 1.

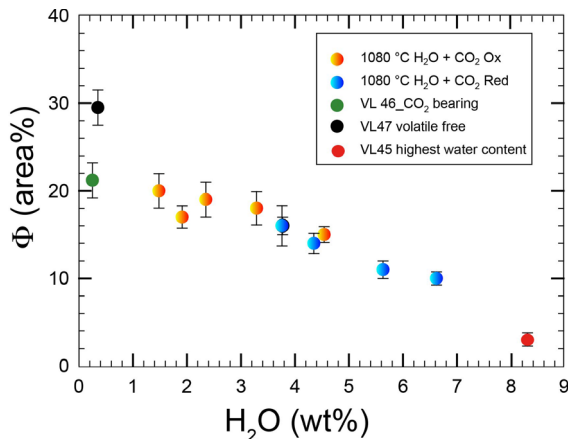


Figure 3. Evolution of crystallinity vs. water content of experiments presented in Table 3. Note the variation on crystallinity between CO₂ bearing and CO₂ free sample in nominally dry experimental charges. Symbols as in Figure 1.

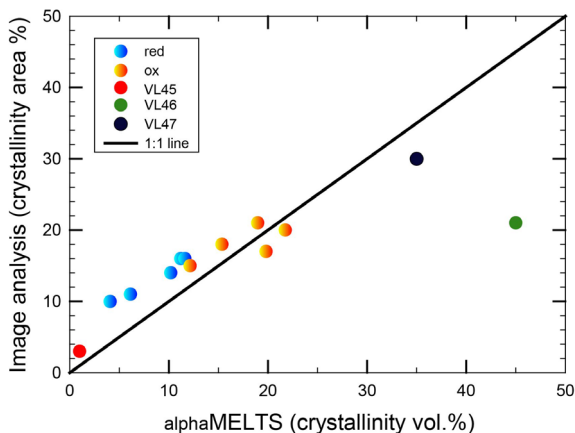


Figure 4. Comparison between Image Analyses measurements and calculated amount of crystals by alphaMELTS approach. Note the good correlation for most of the sample. VL46 sample, instead shows a large departure relatively to the 1:1 line (green circle).

data, although VL46 sample shows a calculated crystallinity higher than 40 vol% (expected from equilibrium thermodynamic calculation) whereas the experimentally observed crystallinity is much lower (Figure 4 and Table 3).

4. Discussion

4.1. Effect of volatiles on phase equilibria

In order to test for equilibrium condition in our experiments we can refer to models proposed by Putirka [2008]. Tests for equilibrium between Cpx and a coexisting liquid can be made by comparing observed and predicted values for Fe–Mg exchange, or $K_D(\text{Fe–Mg})^{\text{cpx-liq}}$, which should be 0.28 ± 0.08 for Cpx (Putirka,2008; considering $\text{FeO}=\text{FeO}_{\text{tot}}$). Our results show values ranging from 0.236 and 0.248 when using compositions in Table 2, indicating compositions close to equilibrium.

The glasses of our isothermal experiments show geochemical trends that are entirely controlled by the degree of crystallinity that itself depends on the composition and amount of volatiles in the system. The evolution trends for most of the elements (Ca, Mg, Si, Al) are consistent with the crystallization of Cpx (Figure 2), which predominates the solid phase. Ti is almost constant in experiments performed at reduced conditions whereas its abundance is lower in the experiments performed under oxidized conditions, due to the crystallization of Fe–Ti oxides in the latter. The composition of melts from two experiments (VL46 and VL47 at very low H₂O content; Tables 2 and 3) deviates slightly from the general trend for some elements and can be explained by the presence of Pl in the run products (Figure 5).

The amount of CO₂ that can be dissolved in melts is lower than that of H₂O and the solubility of both volatiles has been investigated as a function of pressure in a variety of melt compositions [e.g., Brooker *et al.*, 2001, King and Holloway, 2002, Holloway and Blank, 1994, Dixon and Stolper, 1995, Dixon *et al.*, 1995, Jakobsson, 1997, Morizet *et al.*, 2010, Baker and Alletti, 2012, Schanofski *et al.*, 2019]. Carbon species (CO₂, CH₄, and CO) have low solubility in basalt and shoshonite melts [at 500 MPa < 4500 ppm CO₂, Shishkina *et al.*, 2014, Vetere *et al.*, 2014, Behrens *et al.*, 2009, Botcharnikov *et al.*, 2006] and carbonate minerals are not stable in mafic melts. It could therefore be anticipated that (for low CO₂ melt concentrations) CO₂ has no effect on phase compositions and proportions when compared to CO₂-free dry systems. Indeed, samples with high water contents do not show any important differences in terms of crystallinity between CO₂-bearing and CO₂-free samples (Figure 3). This indicates that water plays the most

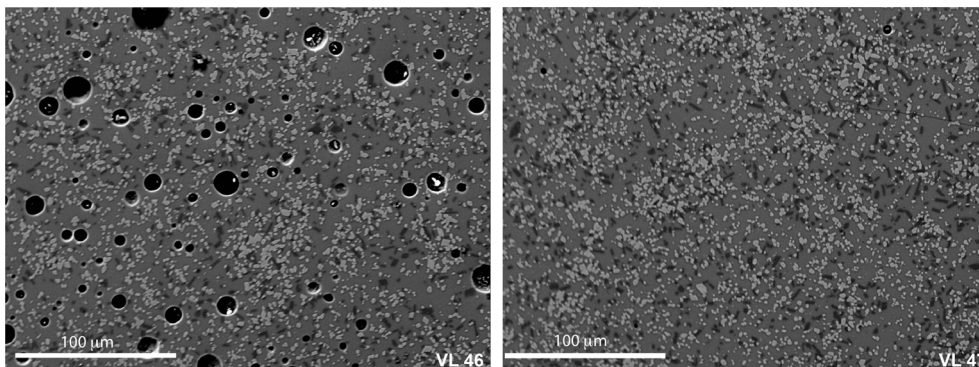


Figure 5. BSE images of sample VL46 and VL47 (see Table 3) after annealing at 1080 °C and pressure of 500 MPa. In particular, as 2.8 wt% CO₂ is added to the system, the crystal content decreases by about 10 area%, and also the relative amount of single crystal phases (Cpx and Pl) decreases (VL46*, Table 3). Clinopyroxene amount varies from 21.6 to 15.1 area% while plagioclase slightly decreases from 8.8 to 5.9 area% (VL46* and VL47*, Table 3).

important role on controlling the crystallization temperatures and that the role of minor to moderate CO₂ concentrations is subordinate. However, for systems with low water and relatively high CO₂ levels, this observation seems not to be valid. The difference of 10% in crystallinity found between nominally dry samples (fluid absent and pure CO₂ fluid) implies that CO₂ does not behave as a fully inert component, only reducing water activity. Following the determinations of Husen *et al.* [2016], it is emphasized that the melts synthesized at nominally dry fluid-absent conditions in the internally-heated pressure vessel used at Hannover probably contain at least 0.5 wt% H₂O. Absolutely dry conditions can never be realized because entrapment of adsorbed water during capsule preparation cannot be avoided and because hydrogen can diffuse through the capsule material at high temperature. This process is partially related to reduction of ferric iron to ferrous iron in the melt during the high *T*-*P* experiments following the reaction



where *m* refers to the melt phase and *g* the gas phase. Thus, the difference between fluid-absent and fluid-present experiments can be considered as a minimum value and may be even larger than determined in this study, if absolutely H₂O-free systems are considered.

Although experimental conditions are very different, our observations are in agreement with

observations of Fiege *et al.* [2015] showing that the addition of ~2000 ppm of CO₂ to a hydrous basaltic melt (5 wt% H₂O) has a small effect on crystal content (Cpx, Spl) and glass fractions (during decompression). Nevertheless, when evaluating in detail those data, we can see that samples containing only H₂O show relatively higher abundance of Cpx compared to those containing both H₂O and CO₂. Experiments simulating the effects of CO₂ fluxing conducted by Giuffrida *et al.* [2017] also indicate that the addition of CO₂ to a partially crystallized basalt can influence the phase proportion and result in a partial dissolution of Cpx, in contrast to the common assumption. Vetere *et al.* [2015b] noted that the crystallinity of Etna basalt decreases as CO₂ is added to the system, which is in agreement with the data from this study on a shoshonitic system. In particular, in those experiments, Pl was the most abundant mineral phase, but Pl was absent when only CO₂ was added to the experimental charge. In addition, CO₂ appeared to lower Cpx abundance [Vetere *et al.*, 2015b]. Thus, CO₂ may not act as a complete inert phase in mafic systems in which it is mainly incorporated as carbonate species.

A closer look on data presented in Figure 3 allows us to further discuss the effect of the CO₂ in magmatic systems. In fact, Figure 3 shows, at least for added water content higher than 2 wt%, a nearly linear correlation between crystallinity and added water content, independently on *f*O₂. In Figure 6 we

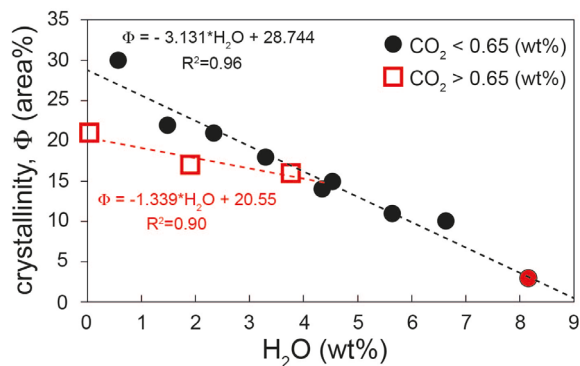


Figure 6. Insight on the evolution of crystallinity vs. water content of experiments presented in Table 3. Note the variation on crystallinity (red and black dashed curves) between samples having water content lower than 3.5 wt% with $\text{CO}_2 > 0.65$ wt% and $\text{CO}_2 < 0.65$ wt%. Equations curves are also reported.

show that, if the amount of added CO_2 is larger than 0.65 wt% and added water content is close or lower than 2 wt%, the crystallinity of the run products becomes lower than what would be predicted from the nearly linear trend between crystallinity and added water, as highlighted by the dashed black and red lines (Figure 6).

More in details, the flushing experiment performed by Giuffrida *et al.* [2017], showed that a CO_2 -rich fluid phase leads to an increase of the amount of Cpx and a decrease of the abundance of Pl at 300 MPa. This decrease of Pl proportion is associated with a change in An content. Although the conditions are very different, as described above, this proves an effect of CO_2 on phase stability. Even if small, we also observed a change in An content from CO_2 free to CO_2 bearing (VL46 to VL47) as observed in Giuffrida *et al.* [2017] from high to low pressure experiments on Etna basalt. The glass compositions presented in Table 2 also highlight some differences between VL46 and VL47 samples. The SiO_2 and Al_2O_3 concentrations are lower in VL46 whereas FeO and CaO concentrations are higher in VL46. This leads to a small variation of NBO/T (0.33 to 0.28) but could mirror the small mineral chemistry variations that we observed. Finally, a liquidus temperature depression, caused by dissolved CO_2 in melt, is expected and this depression may range from negligible to several

hundred degrees depending on silicate melts composition and pressure [Eggler, 1975, 1976, Mysen and Boettcher, 1975, Eggler and Kadik, 1979, Eggler and Rosenhauer, 1978, Boettcher *et al.*, 1987, Boettcher, 1984]. The extent of this depression is linked to the solubility and solubility mechanism(s) of CO_2 in the melt. For instance, the liquidus temperature depression of the $\text{CaMgSi}_2\text{O}_6\text{-CO}_2$ system compared to the volatile free system illustrates this mechanism [Eggler and Rosenhauer, 1978, Mysen and Richet, 2005].

Finally, it is emphasized that the difference in liquidus temperature for the CO_2 bearing and CO_2 free compositions (samples VL46 and VL47) observed experimentally at 500 MPa could not be reproduced with alphaMELTS, with T_L of 1223 °C and 1231 °C, respectively. Thus, the application of thermodynamic models to predict the role of high CO_2 concentrations on phase stability in water-poor systems needs to be reconsidered. This appears to be particularly relevant in Italian volcanic systems, which are often reacting with carbonates.

4.2. Implications for magma dynamics

The data presented above (literature data and our new experimental results) can have profound implications upon the rheological behavior of magmas. In particular, viscosity is highly influenced by the amount of solid phases. This, in turn, might influence the way magma ascends towards the Earth surface and eventually erupts.

The Vulcanello peninsula formed by effusions from a 600 m long, 0.5 to 1.5 m wide eruptive fissure (dike) [Vetere *et al.*, 2007, and reference therein]. Based on the analysis of fluid inclusions in quartz xenoliths we assume for the storage of the shoshonitic magma a trapping depth between 21.5 and 17 km (corresponding to the Moho depth) [Zanon *et al.*, 2003, Peccerillo *et al.*, 2006]. As such, a possible deep storage reservoir could be hypothesised from which, during the eruptive phase of Vulcanello 1, the magma moved directly to the surface, without intermediate storage into the crust [Davì *et al.*, 2009, Nicotra *et al.*, 2018]. Taking into account the water free samples VL46 and VL47 (Figure 5), having a crystal content of about 20 and 30 area%, respectively, we can calculate the effective viscosity of the crystal bearing system using the models

proposed by Sato [2005] and Vona *et al.* [2011] [$\eta_r = \eta_{\text{eff}}/\eta_m$ where η_r is the relative viscosity, η_{eff} is the effective viscosity of the liquid containing a fraction of crystals, and η_m is the viscosity of the melt using the model of Vetere *et al.*, 2007]. Moreover, as required by the Vona *et al.* [2011] model, using image analysis technique on BSE images collected after experiments, one can extract and characterize the crystal shapes from the input grey-scale slides, without considering the possible presence of nanometric crystals [Cassetta *et al.*, 2023]. Procedures are described in Dellino and La Volpe [1996] and Loncaric [1998]. The aspect ratio (AS = major axis/minor axis) parameter providing information on the particles elongation was determined following [Cox and Budhu, 2008]. Results indicate that for our experiments the average AS for Pl is 2.5 and for Cpx is 1.7 while Fe–Ti oxides (when present) have AS close to 1. By taking into account these results, viscosity values of $10^{4.0}$ – $10^{4.4}$ Pa·s are obtained for system containing 20 and 30 area% of crystals, respectively by using the Vona *et al.* [2011] model. These values are comparable to those obtained using the model proposed by Sato [2005, *i.e.* $10^{3.9}$ and $10^{4.2}$ Pa·s].

Figure 7 shows the variation of viscosity of the shoshonitic magma as a function of the crystal and volatile contents. The increase in viscosity is clearly related to the decrease of the volatile content and the relative increase of solid phases.

Considering that magma ascent in dykes is strongly conditioned by dyke width, magma ascent in narrow dykes could be obstructed by magma crystallization. Critical dyke widths were calculated by Petford *et al.* [1994] for magma with felsic composition showing similar viscosities as those investigated here [see also Scaillet *et al.*, 1996]. Results show that dykes thinner than 1 m can hardly propagate from very large depths. We are aware that narrow dykes (<1 m) cannot be approximated to a smooth tabular shape with a constant dyke width, due to the natural roughness of rock fracture planes. However, by doing the identical exercise as in Petford *et al.* [1994], and taking into account (a) basaltic magma temperature, (b) freezing point, (c) rock country temperature (1200 °C, 700 °C and 300 °C respectively), (d) the latent heat for basalt (400 J/g) and (e) the specific heat of basaltic magma ($1.0 \text{ J}\cdot\text{g}^{-1}\cdot\text{°C}^{-1}$), the critical size for dikes reduces to 0.3 m. Thus, we have some constrains for the following discussion.

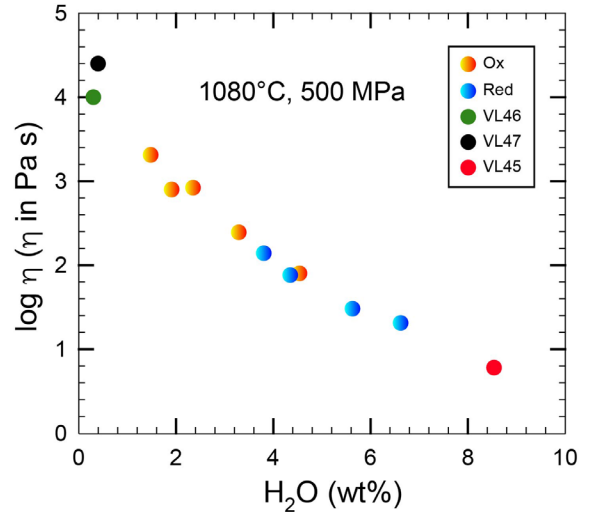


Figure 7. Variation of viscosity vs. water content for samples reported in Table 3. Symbols are identical to those reported in Figures 2 and 3 (see text for details).

In order to calculate a possible ascent velocity (u ; $\text{m}\cdot\text{s}^{-1}$) of these magmas we can use the relation of Lister and Kerr [1991] for laminar flow:

$$u = (w^2/3\eta)\Delta\rho g. \quad (4)$$

As stated above, the eruptive fissure at Vulcanello has width ≤ 1.5 m. If now we consider a density contrast between magma and country rock of $\Delta\rho = 275 \text{ kg}\cdot\text{m}^{-3}$ as reported in Vetere *et al.* [2007], and $\eta = 10^{3.5}$ Pa·s for a system containing melt with 0.3 wt% H₂O (see also Table 3 samples VL46, VL47), we can estimate a possible rise velocity of such magmas, assuming that the width of the conduits varies from 0.1 to 1.5 m. Results are presented in Figure 8a where the ascent velocity is found to vary in the range $u(\text{CO}_2 \text{ free}) = 1.5 \times 10^{-4}$ – 3.5×10^{-2} m/s, and $u(\text{CO}_2 \text{ bearing}) = 5.7 \times 10^{-4}$ – 1.3×10^{-1} m/s. The estimated velocity is subject to an abrupt increase if we consider H₂O–CO₂ bearing systems. Considering that at Vulcanello the water content is estimated between 0.3 and 1.9 wt% [analysis of melt inclusions from shoshonitic samples of Vulcanello in Gioncada *et al.*, 1998 and Clocchiatti *et al.*, 1994a,b] and considering a temperature of 1080 °C [the estimated temperature for Vulcanello magmas is 1083 ± 40 °C, Zanon *et al.*, 2003], a crystallinity of 17 area% can be expected for H₂O- and CO₂-bearing samples (*e.g.* VL37; Table 3). At these

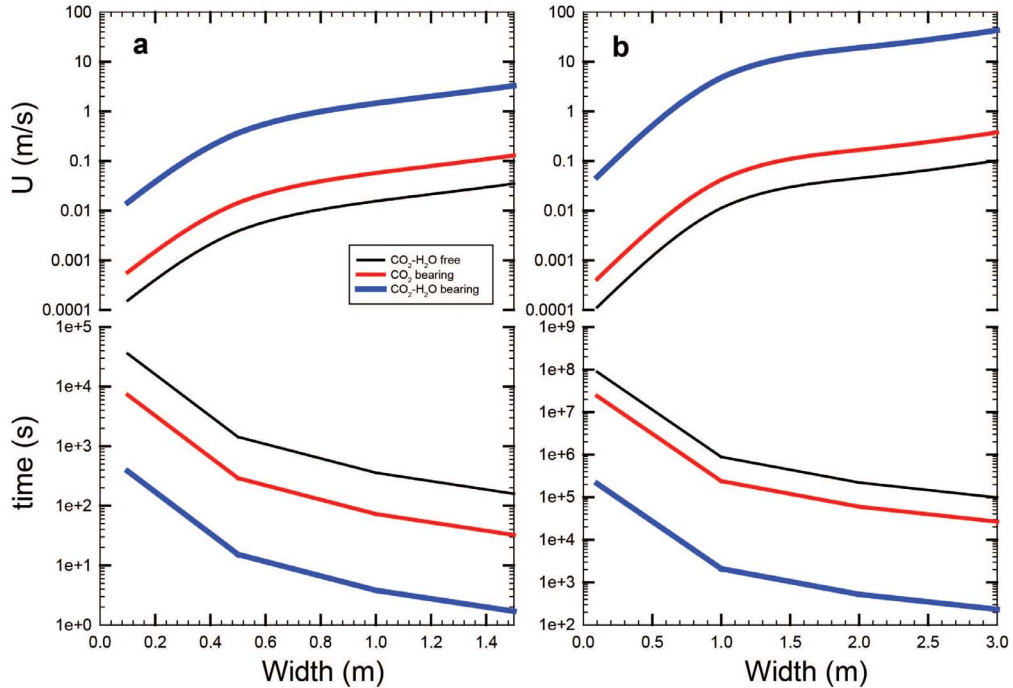


Figure 8. (a,b) Velocities and ascent times evolution vs. conduits size for Vulcanello (a) and hypothetical volcanic systems with dike widths ≤ 3 m and a density contrast between magma and country rock $\Delta\rho = 200 \text{ kg/m}^3$ (b). Please refer to text for details.

conditions the magma viscosity is about $10^{2.8}$ Pa-s and its ascent velocity (1.5×10^{-2} – 3.3 m/s as w varies from 0.1 to 1.5 m, respectively, Figure 7) would be faster than in a volatile-free magma (see $u(\text{CO}_2 \text{ free})$ given above). Thus, in case of a nominally dry magmatic system rising in conduits having width 1.5 m, the time to reach the surface starting from a depth of 20 km is slightly lower than 4 years. However, if CO_2 is present, this duration decreases to ~ 300 days, and < 2 h are estimated assuming that 2.0 wt% H_2O + 0.6 wt% CO_2 are dissolved in the melt. Although these short timescales cannot be applied to the Vulcanello magma, which has lower volatile [Clocchiatti *et al.*, 1994a,b], they could be relevant to other shoshonitic volcanic systems.

As a further example, by making identical considerations as above, we can consider a hypothetical scenario with a viscosity $\eta = 10^{3.5}$ Pa-s (for a system containing melt + 0.3 wt% H_2O see Table 3, samples VL46, VL47). Thus, if dyke widths are ≤ 3 m and the density contrast between magma and country rock is $\Delta\rho = 200 \text{ kg/m}^3$ and adopting Equation (4), we can have an estimate of the possible rise velocity as pre-

sented in Figure 8b. In this case, results are: $u(\text{CO}_2 \text{ free}) = 1.1 \times 10^{-4}$ – 1.0×10^{-1} m/s, and $u(\text{CO}_2 \text{ bearing}) = 4.2 \times 10^{-4}$ – 3.7×10^{-1} m/s. Finally, if we consider H_2O – CO_2 bearing systems with concentrations similar to the experiments VL32 or VL33 (Table 3) and a temperature of 1080 °C, the lower crystallinity allows magma to have viscosity in the order of 10^2 Pa-s and, as consequence, to rise much faster in the range 4.7×10^{-2} – 42.9 m/s as w varies from 0.1 to 3 m, respectively (Figure 8). It is important to keep in mind that in dynamic magmatic systems (during ascent) the CO_2 release is relatively rapid and possibly can locally accelerate magma ascent.

5. Conclusions

Crystallization experiments of a natural shoshonite were performed at 500 MPa, and 1080 °C and water activities $a_{\text{H}_2\text{O}}$ from 0.01 to 1.00. Results show that clinopyroxene is the main crystallizing phase and plagioclase is found to be a stable phase only for water activity lower than 0.1, while spinel is present

in all the runs except in those where $\log f_{\text{O}_2}$ was lower than -9 ($\Delta\text{NNO} = -0.11$).

Interestingly, at low water activity (below 0.1) the addition of CO_2 at constant water content reduces the crystallinity of shoshonitic systems. This behaviour is not predicted by classical thermodynamic models. Thus, in the case of CO_2 -rich and H_2O -poor systems, magmas become less viscous due to the relative decrease in crystallinity. The application of viscosity models to our experimental dataset allows us to infer the possible ascent velocity and ascent time of this type of shoshonitic H_2O -poor magmas from Vulcanello.

Since the magmatic composition used for our study is chemically similar to many Italian volcanic systems (Aeolian Arc, Campi Flegrei, Ischia Island, Pontine Islands, Monti Cimini, Monte Amiata, Capraia Island, Radicofani, Roccamonfina) and also to other systems worldwide (Yellowstone, Mariana Arc, Kurile Arc, Tonga Arc, Andean Arc, Kamchatka Arc), we suggest that our observations will be useful to better understand shoshonitic magma behaviour under relevant geological scenarios. The probability of very rapid ascent of less-evolved melts from depth has to be taken into account for future volcanic crisis and hazard evaluation.

Conflicts of interest

Authors have no conflict of interest to declare.

Acknowledgements

This study was funded by the “Piano di Sostegno alla Ricerca 2022 per finanziamenti a progetti di ricerca Curiosity-driven (F-CUR_CREAMI)” to FV.

References

- Angell, C. A. (1995). Formation of glasses from liquids and biopolymers. *Science*, 267, 1924–1935.
- Arrighi, S., Tanguy, J. C., and Rosi, M. (2006). Eruptions of the last 2200 years at Vulcano and Vulcanello (Aeolian Islands, Italy) dated by high-accuracy archeomagnetism. *Phys. Earth Planet. Inter.*, 159, 225–233.
- Asimow, P. D. and Ghiorso, M. S. (1998). Algorithmic modifications extending MELTS to calculate sub-solidus phase relations. *Am. Mineral.*, 83, 1127–1132.
- Baker, D. R. and Alletti, M. (2012). Fluid saturation and volatile partitioning between melts and hydrous fluids in crustal magmatic systems: The contribution of experimental measurements and solubility models. *Earth Sci. Rev.*, 114, 298–324.
- Behrens, H., Misiti, V., Freda, C., Vetere, F., Botcharnikov, R. E., and Scarlato, P. (2009). Solubility of H_2O and CO_2 in ultrapotassic melts at 1200 and 1250 °C and pressure from 50 to 500 MPa. *Am. Mineral.*, 94, 105–120.
- Berndt, J., Liebske, C., Holtz, F., Freise, M., Nowak, M., Ziegenbein, D., Hurkuck, W., and Koepke, J. (2002). A combined rapid-quench and H_2 -membrane setup for internally heated pressure vessels: Description and application for water solubility in basaltic melts. *Am. Mineral.*, 87, 1717–1726.
- Boettcher, A. L. (1984). The system $\text{SiO}_2\text{--H}_2\text{O--CO}_2$: melting solubility mechanisms of carbon and liquid structure to high pressures. *Am. Mineral.*, 69, 823–834.
- Boettcher, A. L., Luth, R. W., and White, B. S. (1987). Carbon in silicate liquids: the systems $\text{NaAlSi}_3\text{O}_8\text{--CO}_2$, $\text{CaAl}_2\text{Si}_2\text{O}_8\text{--CO}_2$, and $\text{KAlSi}_3\text{O}_8\text{--CO}_2$. *Contrib. Mineral. Petrol.*, 97, 297–304.
- Botcharnikov, R. E., Behrens, H., and Holtz, F. (2006). Solubility and speciation of C–O–H fluids in andesitic melt at $T = 1100\text{--}1300$ °C and $P = 200$ and 500 MPa. *Chem. Geol.*, 229, 125–143.
- Botcharnikov, R. E., Freise, M., Holtz, F., and Behrens, H. (2005). Solubility of C–O–H mixtures in natural melts: New experimental data and application range of recent models. *Ann. Geophys.*, 48, 633–646.
- Brooker, R. A., Kohn, S. C., Holloway, J. R., and McMillan, P. F. (2001). Structural controls on the solubility of CO_2 in silicate melts Part I: bulk solubility data. *Chem. Geol.*, 174, 225–239.
- Burnham, C. W. (1981). The nature of multicomponent aluminosilicate melts. In Rickard, D. T. and Wickman, F. E., editors, *Chemistry and Geochemistry of Solutions at High Temperatures and Pressures*, pages 197–229. Pergamon Press, New York.
- Cassetta, M., Vetere, F., Zanatta, M., Perugini, D., Alvaro, M., Giannetta, B., Zaccone, C., and Daldosso, N. (2023). Micro-Raman spectroscopy for a comprehensive understanding of the structural evolution of Basaltic-Andesite and Trachybasalt multiphase systems. *Chem. Geol.*, 616, article no. 121241.

- Clemens, J. D. and Wall, V. J. (1981). Origin and crystallization of some peraluminous (S-type) granitic magmas. *Can. Mineral.*, 19, 111–131.
- Clocchiatti, R., Del Moro, A., Gioncada, A., Joron, J. L., Mosbah, M., Pinarelli, L., and Sbrana, A. (1994a). Assessment of a shallow magmatic system: the 1888–1890 eruption, Vulcano Island, Italy. *Bull. Volcanol.*, 56, 466–486.
- Clocchiatti, R., Gioncada, A., Mosbah, M., and Sbrana, A. (1994b). Possible deep origin of sulfur output at Vulcano (southern Italy) in the light of melt inclusions studies. *Acta Vulcanol.*, 5, 49–54.
- Cox, M. R. and Budhu, B. (2008). A practical approach to grain shape quantification. *Eng. Geol.*, 96, 1–16.
- Davì, M., De Rosa, R., Donato, P., Vetere, F., Barca, D., and Cavallo, A. (2009). Magmatic evolution and plumbing system of ring-fault volcanism: the Vulcanello Peninsula (Aeolian Islands, Italy). *Eur. J. Mineral.*, 21, 1009–1028.
- De Astis, G., Lucchi, F., Dellino, P., La Volpe, L., Tranne, C. A., Frezzotti, M. L., and Peccerillo, A. (2013). Geology, volcanic history and petrology of Vulcano (central Aeolian archipelago). *Geol. Soc. Lond. Mem.*, 37(1), 281–349.
- De Ritis, R., Ravat, D., Ventura, G., and Chiappini, M. (2013). Curie isotherm depth from aero-magnetic data constraining shallow heat source depths in the central Aeolian Ridge (Southern Tyrrhenian Sea, Italy). *Bull. Volcanol.*, 75, article no. 710.
- Dellino, P. and La Volpe, L. (1996). Image processing analysis in reconstructing fragmentation and transportation mechanisms of pyroclastic deposits. The case of Monte Pilato-Rocche Rosse eruptions, Lipari (Aeolian islands, Italy). *J. Volcanol. Geotherm. Res.*, 71, 13–29.
- Devine, J. D., Gardner, J. E., Brack, H. P., Layne, G. D., and Rutherford, M. J. (1995). Comparison of microanalytical methods for estimating H₂O contents of silicic volcanic glasses. *Am. Mineral.*, 80, 319–328.
- Dixon, J. E. and Stolper, E. M. (1995). An experimental study of water and carbon dioxide solubilities in Mid-Ocean Ridge Basaltic liquids. Part II: applications to degassing. *J. Petrol.*, 36, 1633–1646.
- Dixon, J. E., Stolper, E. M., and Holloway, J. R. (1995). An experimental study of water and carbon dioxide solubilities in mid-ocean ridge basaltic liquids. Part I: Calibration and solubility models. *J. Petrol.*, 36, 1607–1631.
- Eggler, D. H. (1975). CO₂ as a volatile component in the mantle: the system Mg₂SiO₄–SiO₂–H₂O–CO₂. *Phys. Chem. Earth*, 9, 869–881.
- Eggler, D. H. (1976). Does CO₂ cause partial melting in the low-velocity layer of the mantle? *Geology*, 4(2), 69–72.
- Eggler, D. H. and Kadik, A. A. (1979). The system NaAlSi₃O₈–H₂O–CO₂: I. Compositional and thermodynamic relations of liquids and vapors coexisting with albite. *Am. Mineral.*, 64, 1036–1049.
- Eggler, D. H. and Rosenhauer, M. (1978). Carbon dioxide in silicate melts. II. Solubilities of CO₂ and H₂O in CaMgSi₂O₆ (diopside) liquids and vapors at pressures to 40 kb. *Am. J. Sci.*, 278, 64–94.
- Falsaperla, S., Neri, G., and Velardita, S. (1985). Struttura della crosta superiore dell'area delle isole Eolie. *Rend. Osserv. Geofis. Reggino*, XXIX, 103–111.
- Fiege, A., Vetere, F., Holtz, F., Simon, A., and Iezzi, G. (2015). Crystallization induced by decompression in basaltic system: implication for magma ascent and degassing. *Chem. Geol.*, 411, 310–322.
- Fusillo, R., Di Traglia, F., Gioncada, A., Pistolesi, M., Wallace, P. J., and Rosi, M. (2015). Deciphering post-caldera volcanism: insight into the Vulcanello (Island of Vulcano, Southern Italy) eruptive activity based on geological and petrological constraints. *Bull. Volcanol.*, 77, article no. 76.
- Ghiorso, M. S., Hirschmann, M. M., Reiners, P. W., and Kress III, V. C. (2002). The pMELTS: A revision of MELTS for improved calculation of phase relations and major element partitioning related to partial melting of the mantle to 3 GPa. *Geochem. Geophys. Geosyst.*, 3(5), 1–36.
- Ghiorso, M. S. and Sack, R. O. (1995). Chemical mass transfer in magmatic processes: IV. A revised and internally consistent thermodynamic model for the interpretation and extrapolation of liquid–solid equilibria in magmatic systems at elevated temperatures and pressures. *Contrib. Mineral. Petrol.*, 119, 197–212.
- Gioncada, A., Clocchiatti, R., Sbrana, A., Bottazzi, P., Massare, D., and Ottolini, L. (1998). A study of melt inclusions at Vulcano (Aeolian Islands, Italy): insights on the primitive magmas and on the volcanic feeding system. *Bull. Volcanol.*, 60, 286–306.
- Giordano, D. and Dingwell, D. B. (2003). The kinetic fragility of natural silicate melts. *J. Phys. Condens. Matter*, 15, 945–954.

- Giuffrida, M., Vetere, F., Viccaro, M., and Holtz, F. (2017). The effect of CO₂ flushing on Etnean magmas: an experimental approach. *Contrib. Mineral. Petrol.*, 172, article no. 90.
- Holloway, J. R. and Blank, J. G. (1994). Application of experimental results to C–O–H species in natural melts. In Carroll, M. R. and Holloway, J. R., editors, *Volatiles in Magmas*, volume 30 of *Reviews in Mineralogy*, pages 187–230. Mineralogical Society of America, Chantilly, VA.
- Husen, A., Almeev, R. R., and Holtz, F. (2016). The effect of H₂O and pressure on multiple saturation and liquid lines of descent in basalts from the Shatsky Rise. *J. Petrol.*, 57(2), 309–344.
- Jakobsson, S. (1997). Solubility of water and carbon dioxide in an icelandite at 1400 °C and 10 kilobars. *Contrib. Mineral. Petrol.*, 127, 129–135.
- Jarosewich, E. J. (2002). Smithsonian microbeam standards. *J. Res. Natl. Inst. Stand. Technol.*, 107(6), 681–685.
- Kent, A. J. R. (2008). Melt inclusions in basaltic and related volcanic rocks. In Putirka, K. D. and Tepley III, F. J., editors, *Minerals, Inclusions and Volcanic Processes*, volume 69 of *Reviews in Mineralogy and Geochemistry*, pages 273–331. Mineralogical Society of America and Geochemical Society.
- King, P. L. and Holloway, J. R. (2002). CO₂ solubility and speciation in intermediate (andesitic) melts: The role of H₂O and composition. *Geochim. Cosmochim. Acta*, 66, 1627–1640.
- Li, X., Zhang, C., Almeev, R. R., and Holtz, F. (2020). GeoBalance: An Excel VBA program for mass balance calculation in T geosciences. *Geochemistry*, 80, article no. 125629.
- Lister, J. R. and Kerr, R. C. (1991). Fluid-mechanical models of crack propagation and their application to magma transport in a dyke. *J. Geophys. Res.*, 96, 10049–10077.
- Loncaric, S. (1998). A survey of shape analysis techniques. *Pattern Recognit.*, 31, 983–1001.
- Martel, C., Brooker, R. A., Andújar, J., Pichavant, M., Scaillet, B., and Blundy, J. D. (2019). Experimental simulations of magma storage and ascent. In *Advances in Volcanology*, pages 101–110. Springer, Cham.
- Martel, C., Pichavant, M., Bourdier, J.-L., Holtz, F., and Scaillet, B. (1998). Magma storage conditions and control of eruption regime in silicic volcanoes: experimental evidence from Mt. Pele. *Earth Planet. Sci. Lett.*, 156(1–2), 89–99.
- Morizet, Y., Paris, M., Gaillard, F., and Scaillet, B. (2010). C–O–H fluid solubility in haplobasalt under reducing conditions: an experimental study. *Chem. Geol.*, 279, 1–16.
- Mysen, B. O. and Boettcher, A. L. (1975). Melting of a hydrous mantle. I. Phase relations of natural peridotite at high pressures and temperatures with controlled activities of water, carbon dioxide and hydrogen. *J. Petrol.*, 16, 520–548.
- Mysen, B. O. and Richet, P. (2005). *Silicate Glasses and Melts, Properties and Structure*. Elsevier, Amsterdam.
- Nicotra, E., Giuffrida, M., Viccaro, M., Donato, P., D’Orlando, C., Paonita, A., and De Rosa, R. (2018). Timescales of pre-eruptive magmatic processes at Vulcano (Aeolian Islands, Italy) during the last 1000 years. *Lithos*, 316–317, 347–365.
- Parat, F., Holtz, F., and Feig, S. (2008). Pre-eruptive Conditions of the Huerto Andesite (Fish Canyon System, San Juan Volcanic Field, Colorado): Influence of volatiles (C–O–H–S) on phase equilibria and mineral composition. *J. Petrol.*, 49, 911–935.
- Peccherillo, A., Frezzotti, M. L., De Astis, G., and Ventura, G. (2006). Modeling the magma plumbing system of Vulcano (Aeolian Island, Italy) by integrative fluid-inclusion geobarometry, petrology and geophysics. *Geology*, 34, 17–20.
- Petford, N., Lister, R. J., and Kerr, R. C. (1994). The ascent of felsic magma in dykes. *Lithos*, 32, 161–168.
- Pouchou, J. L. and Pichoir, F. (1991). Quantitative analysis of homogeneous or stratified microvolumes applying the model “PAP”. In *Electron Probe Quantification*, pages 31–75. Springer, Boston, MA.
- Putirka, K. (2008). Thermometers and barometers for volcanic systems. In Putirka, K. and Tepley, F., editors, *Minerals, Inclusions and Volcanic Processes*, volume 69 of *Reviews in Mineralogy and Geochemistry*, pages 61–120. Mineralogical Society of America, Chantilly, VA.
- Sato, H. (2005). Viscosity measurements of subliquidus magmas: 1707 basalt of Fuji volcano. *J. Mineral. Petrol. Sci.*, 100, 133–142.
- Scaillet, B. and Evans, B. W. (1999). The June 15, 1991 eruption of Mount Pinatubo. I. Phase equilibria and pre-eruption P–T–fO₂–fH₂O conditions of the dacite magma. *J. Petrol.*, 40, 381–411.

- Scaillet, B., Holtz, F., Pichavant, M., and Schmidt, M. (1996). Viscosity of Himalayan leucogranites: Implications for mechanisms of granitic magma ascent. *J. Geophys. Res.*, 101, 27691–27699.
- Schanofski, M., Fanara, S., and Schmidt, B. C. (2019). CO₂–H₂O solubility in K-rich phonolitic and leucititic melts. *Contrib. Mineral. Petrol.*, 174, article no. 52.
- Schulze, F., Behrens, H., Holz, F., Ruox, J., and Johannes, W. (1997). The influence of H₂O on the viscosity of a haplogranitic melt. *Am. Mineral.*, 81, 1155–1165.
- Shishkina, T., Botcharnikov, R. E., Holtz, F., Almeev, R. R., Jazwa, A. M., and Jakubiak, A. A. (2014). Compositional and pressure effects on the solubility of H₂O and CO₂ in mafic melts. *Chem. Geol.*, 277, 115–125.
- Sisson, T. W. and Layne, G. D. (1992). H₂O in basalt and basaltic andesite glass inclusions from four subduction-related volcanoes. *Earth Planet. Sci. Lett.*, 117, 619–635.
- Smith, P. M. and Asimow, P. D. (2005). Adibat_1ph: A new public front-end to the MELTS, pMELTS, and pHMELTS models. *Geochem. Geophys. Geosyst.*, 6, article no. Q02004.
- Vetere, F., Behrens, H., Botcharnikov, R., Holtz, F., and Fanara, S. (2014). The role of alkalis in the solubility of H₂O and CO₂ in silicate melts. Implication for phonotephritic magmas. *Contrib. Mineral. Petrol.*, 167, 1–17.
- Vetere, F., Behrens, H., Misiti, V., Ventura, G., De Rosa, R., Holtz, F., and Deubener, J. (2007). Viscosity of shoshonitic melt (Vulcanello Aeolian Islands, Italy) and inference on the dynamics of magma ascent. *Chem. Geol.*, 245, 89–102.
- Vetere, F., Botcharnikov, R. R., Behrens, H., Holtz, F., and De Rosa, R. (2011). Solubility of H₂O and CO₂ in shoshonitic melts at 1250 °C and pressure from 50 to 400 MPa. *J. Volcanol. Geotherm. Res.*, 202, 251–261.
- Vetere, F., Iezzi, G., Behrens, H., Holtz, F., Ventura, G., Misiti, V., Cavallo, A., Mollo, S., and Dietrich, M. (2015a). Glass forming ability and crystallization behaviour of sub-alkaline silicate melts. *Earth Sci. Rev.*, 150, 25–44.
- Vetere, F., Mollo, S., Giacomoni, P. P., Iezzi, G., Coltorti, M., Ferlito, C., Holtz, F., Perugini, D., and Scarlato, P. (2015b). Experimental constraints on the origin of pahoehoe “cicirara” lavas at Mt. Etna volcano (Sicily, Italy). *Bull. Volcanol.*, 77, article no. 44.
- Vona, A., Romano, C., Dingwell, D. B., and Giordano, D. (2011). The rheology of crystal-bearing basaltic magmas from Stromboli and Etna. *Geochim. Cosmochim. Acta*, 75, 3214–3236.
- Zanon, V., Frezzotti, M. L., and Peccerillo, A. (2003). Magmatic feeding system and crustal magma accumulation beneath Vulcano Island (Italy): evidence from fluid inclusions in quartz xenoliths. *J. Geophys. Res.*, 108, 1–13.